Cite as: J. Appl. Phys. 131, 225110 (2022); doi: 10.1063/5.0077441

Submitted: 11 April 2022 · Accepted: 19 May 2022 ·

Published Online: 13 June 2022



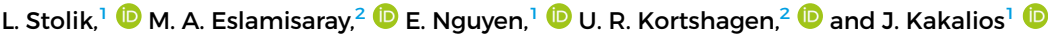


















AFFILIATIONS

¹School of Physics and Astronomy, University of Minnesota, Minneapolis, Minnesota 55455, USA

²Department of Mechanical Engineering, University of Minnesota, Minneapolis, Minnesota 55455, USA

ABSTRACT

Measurements of the dark conductivity and thermoelectric power in hydrogenated amorphous silicon-germanium alloys (a-Si_{1-x}Ge_x:H) reveal that charge transport is not well described by an Arrhenius expression. For alloys with concentrations of Ge below 20%, anomalous hopping conductivity is observed with a power-law exponent of 3/4, while the temperature dependence of the conductivity of alloys with higher Ge concentrations is best fit by a combination of anomalous hopping and a power-law temperature dependence. The latter has been higher Ge concentrations is best fit by a combination of anomaious nopping and a power-law temperature dependence. The latter has been attributed to charge transport via multi-phonon hopping. Corresponding measurements of the Seebeck coefficient reveal that the thermopower is n-type for the purely a-Si:H and a-Ge:H samples but that it exhibits a transition from negative to positive values as a function of the Ge content and temperature. These findings are interpreted in terms of conduction via hopping through either exponential band tail states or dangling bond defects, suggesting that the concept of a mobility edge, accepted for over five decades, may not be necessary to account for charge transport in amorphous semiconductors.

Published under an exclusive license by AIP Publishing. https://doi.org/10.1063/5.0077441

I. INTRODUCTION

Interest in amorphous semiconductors stems in part from their use in applications that do not require the high electronic mobility of single crystal materials but rather call for electronic materials to cover large surface areas on a variety of substrate surfaces at low cost. 1-3 To list just a few examples, the ubiquity of light-weight, low-power flat panel liquid crystal displays is due in part to advances in the fabrication of hydrogenated amorphous silicon (a-Si:H) based thin-film transistors, employed to modulate the optical properties of the large array of liquid crystal pixels.⁴ Xerography^{5,6} and medical x-ray imaging⁷ also make use of the large-area advantages of thin-film semiconductors, and amorphous semiconductors are promising candidate materials for high-energy particle detectors and satellite-based solar cells as their random atomic arrangements lead to them being less susceptible to damage following exposure to ionizing radiation than crystalline semiconductors.^{8–10} Photovoltaic devices require large surface areas to maximize solar absorption, and while a-Si:H-based solar cells have lower conversion efficiencies than crystalline Si-based photovoltaics as well as stability issues, they can be easily deposited on a wide range of substrates (as there are no lattice matching constraints) over large areas at any desired thickness. 11,12 The optical gap of a-Si:H can be varied by alloying with germanium or carbon,

making these alloys attractive for large-area thin-film photovoltaic applications. One technique adopted to work around the stability issue is to fabricate a-Si:H-based tandem cells, where an a-Si:H solar cell is sandwiched between solar cells composed of amorphous alloys of silicon-carbon and silicon-germanium, having larger and smaller bandgaps, respectively, compared with a-Si:H 13 larger and smaller bandgaps, respectively, compared with a-Si:H.¹³

One of the most basic but also striking characteristics of charge transport in amorphous semiconductors is the observation that the temperature dependence of the dark conductivity is consistent with a simple, thermally activated expression, where the activation energy is approximately half of the optical gap. While a \frac{1}{24} thermally activated conductivity in crystalline semiconductors is attributed to a gap in the density of states between the valence and the conduction bands, in amorphous semiconductors, there is a continuous distribution of states between the highest energy occupied level and the lowest energy unoccupied level. In these strongly disordered materials, the thermally activated conductivity is instead ascribed to the presence of a "mobility gap" separating localized and extended states, first proposed by Sir Neville Mott in 1967. 14 However, recent studies have found that the conductivity of undoped¹⁵ and n-type doped a-Si:H, ¹⁶ as well as composite films of a-Si:H containing nanocrystalline inclusions of either silicon or germanium (nc-Si or nc-Ge), 15 is not, in fact, thermally activated, but

rather is best described by an anomalous hopping expression

$$\sigma(T) = \sigma_1 \exp\left[-\left(\frac{T_o}{T}\right)^{\kappa}\right],\tag{1}$$

where σ is the electrical conductivity, T is the temperature, T_{σ} is a characteristic temperature, σ_1 is the pre-exponential factor, and the exponent $\kappa \sim 0.75 \pm 0.05$. This $\kappa = 3/4$ temperature dependence has also been found to describe the low-temperature conductivity of ultra-thin disordered films of Ag, Bi, Pb, and Pd, 17 twodimensional electron systems in high parallel magnetic fields, 18,19 ultra-thin quench condensed Bi films,²⁰ carbon-black polymer composites,²¹ weakly coupled Au nanoparticles,²² and ZnO quantum dot arrays.²³ There is no accepted theoretical model for this conductivity temperature dependence.

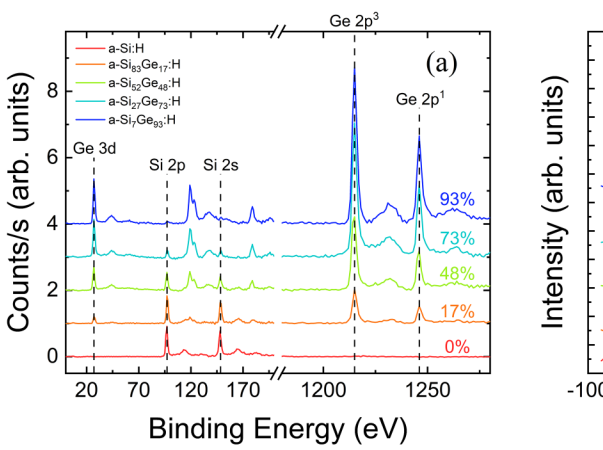
These observations raise the question as to whether this temperature dependence is observed in other amorphous semiconductors. In this paper, we report measurements of the temperature dependence of the dark conductivity of a series of undoped hydrogenated amorphous silicon-germanium alloys, where the Ge content is varied from 0% (pure a-Si:H) to 100% (pure a-Ge:H). We find that for low Ge concentrations, anomalous hopping is observed, while for higher Ge concentrations, the dark conductivity below room temperature displays a power-law dependence on temperature, suggesting that charge transport proceeds via multiphonon hopping. That conduction takes place, at least in part, through hopping via midgap defects even above room temperature is consistent with the measurements of the Seebeck coefficient in these films, reported below.

This paper is organized as follows. Section II presents an overview of sample preparation and structural characterization, along with the dark conductivity, thermopower, and photoconductivity measurement procedures. The results of conductivity, Seebeck coefficient, and photoconductivity measurements are presented in Sec. III. A model to explain the high and low-temperature conductance and thermopower results is discussed in Sec. IV Finally, features of the charge transport mechanisms in the amorphous silicon-germanium alloys are summarized in Sec. V.

II. EXPERIMENTAL METHODS AND SAMPLE **CHARACTERIZATION**

Hydrogenated amorphous silicon-germanium (a-Si_{1-x}Ge_x:H) thin films were synthesized in a plasma enhanced chemical vapor deposition (PECVD) reactor, where a low-temperature plasma was employed to dissociate silane (SiH₄) and germane (GeH₄) precursors dynamically mixed with a carrier gas, argon (Ar). By varying the silane to germane ratio injected into the chamber, we deposited a series of a-Si_{1-x}Ge_x:H thin films, with $0 \le x \le 1.0$, onto low ion-impurity quartz substrates maintained at 520 K during film growth. An RF power of 4W at 13.56 MHz (an electrode area of 62.2 cm² and an electrode separation of 2.4 cm) was applied at a chamber pressure of 220 mTorr. The films' thicknesses, determined using a KLA-Tencor P-7 stylus profiler, are $\sim 2 \,\mu\text{m}$, except for the pure a-Si:H film, the thickness of which is $0.85 \,\mu\text{m}$, and for the a-Ge:H film, which is $0.33 \,\mu m$ thick. Coplanar aluminum electrodes of thickness 150 nm, length 10 mm, and electrode separation of 4 mm were deposited across the surface of the sample following deposition. These electrodes yielded linear current-voltage characteristics at all temperatures investigated.

As the Ge/Si ratio incorporated into the growing amorphous film differs from the GeH₄/SiH₄ ratio used in the reactor chamber,²⁴ it is important to independently determine the precise stoichiometry of the films. The Ge and Si content of the alloy thin films was determined via x-ray photoelectron spectroscopy (XPS), as shown in Fig. 1(a). The films studied here were determined to have germanium concentrations of x = 0, 0.17, 0.48, 0.73, 0.93, and 1.0. The relative Si and Ge content was further confirmed through Raman spectroscopy, where the LO and TO modes of silicon and germanium are detected. Raman spectra for the a-Si_{1-x}Ge_x:H film series, shown in Fig. 1(b), was measured using a 514.5- nm argon repair of the a-Si_{1-x}Ge_x:H film series, shown in Fig. 1(b), was measured using a 514.5- nm argon repair of the a-Si₁Ge_x:H mined via x-ray photoelectron spectroscopy (XPS), as shown in $\frac{\overline{\Omega}}{\Phi}$



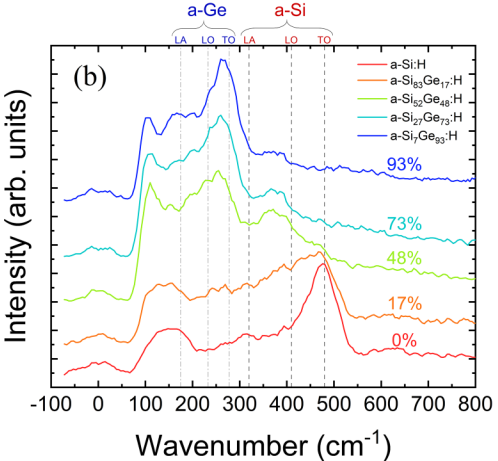


FIG. 1. (a) X-ray photoelectron and (b) Raman spectra of a-Si_{1-x}Ge_x:H film series showing the composition of amorphous thin films with different Ge concentrations.

ion laser focused to a spot size of $\sim 0.3 \,\mu \mathrm{m}$ in diameter at a power of less than 6 mW, with care taken to avoid crystallization of the films. As expected, there is an appreciable reduction of the Si-Si TO mode (at ~476 cm⁻¹) and an increase of the Ge-Ge TO mode (at ~269 cm⁻¹) as the Ge concentration determined by XPS increases. Moreover, the peak corresponding to the SiGe mode (at \sim 371 cm⁻¹) appears in samples with the Ge/Si ratio near 50/50.

The dark conductivity was measured in a closed-cycle He cryostat, capable of maintaining stable temperatures from 10 to 500 K at a pressure below 1 mTorr. The highest temperature employed was ~500 K, in order to stay below the deposition temperature of 520 K at which the films were synthesized. Annealing at or above the deposition temperature induces irreversible changes in the electronic properties of a-Si:H, while the lower temperatures are limited by the current that can be reliably measured. A DC voltage of up to 100 V was applied across the coplanar electrodes and the current was measured by using a femto-ammeter. As the samples presented here were all undoped and very resistive, with room temperature resistances between $1 G\Omega$ and $100 T\Omega$, any contact resistances that may be present at the interfaces between the sample and the electrodes, expected to be less than a few hundred Ohms, are negligible in our final current measurements. All samples were first annealed at 470 K in the dark under vacuum (annealed state A) to remove any effects due to prior light exposure (the Staebler-Wronski effect²⁵) or surface adsorbates such as water vapor²⁶ could induce a surface charge and band bending in thin films.

Deviations from Arrhenius behavior were determined through a reduced activation energy analysis technique. In this procedure, developed by Zabrodskii and Shlimak,²⁷ the logarithmic derivative of the conductivity $W(T) = \frac{d \ln \sigma}{d \ln T}$ is computed and plotted against temperature on a log-log plot. A conductivity temperature dependence of the form of Eq. (1) will result in a straight line of slope κ . Known κ values could be due to thermally activated conduction ($\kappa = 1$), Efros-Shklovskii variable range hopping ($\kappa = 1/2$), ²⁸ Mott variable range hopping ($\kappa = 1/4$),²⁹ or for $\kappa = 0$, a power-law temperature dependence ($\sigma \sim T^n$ where n > 1) that is often ascribed to multi-phonon hopping processes.

Measurements of the Seebeck coefficient were performed in a custom-made system. Inside a vacuum chamber capable of reaching ~30 mTorr, the sample was placed across two copper blocks 4 mm apart such that the sample's deposited coplanar electrodes were directly above the edges of the copper blocks. A 50 W cartridge heater is embedded within each Cu block. The temperatures of the blocks T_1 and T_2 were set so that the average is $T_{avg} = \frac{T_1 + T_1}{2}$ and the temperature gradient is $\Delta T = T_1 - T_2$. The temperature equilibration times were sufficiently long (2 min) to ensure a uniform temperature between the blocks and the sample surface. The temperature gradient set across the sample electrodes induced a thermoelectric voltage $(\Delta V = V_1 - V_2)$ across the sample. For each average temperature, thermal gradients ΔT varying from ± 8 with 1 K intervals were generated, and the respective induced voltages were recorded, eliminating contributions of any small temperature-dependent voltage offset to the signal. The Seebeck coefficient is defined as

$$S = \frac{\Delta V}{\Delta T},\tag{2}$$

which was obtained from the slope of the linear plot of induced voltage against ΔT , in this case ranging from -8 to 8 K. The process was then repeated at a new average temperature, from 320 to 480 K.

Measurements of the photoconductivity were performed in a system similar to that used for the dark conductivity measurements. The sample was annealed and cooled down to room temperature, after which the photoconductivity was measured using a heat-filtered W-Halogen lamp (intensity ~75 mW/cm²). The steady state photoconductivity was then defined as the difference between the measured photoconductivity and the dark conductivity. The sensitivity of the room temperature photoconductivity of the a-Si_{1-x}Ge_x:H thin films to the white light intensity was also investigated using a series of neutral density filters, starting with the lowest light intensity.

III. DARK CONDUCTIVITY

shown in Fig. 2. At first glance, the conductivity can be fit reasonably well with a simple thermally activated expression over the range of 300 to 470 K, particularly for films with lower Ge concentrations. For films with a germanium concentration above 50% deviations from a simple, thermally activated conductivity are evident at low temperatures. However, a reduced activation energy analysis indicates that even the pure a-Si:H and a-Si₈₃Ge₁₇:H films are not best described by an Arrhenius expression.

Figure 3(a) shows a log-log plot of the Zabrodskii reduced activation energy against temperature for all samples. Similar results were obtained for measurements on additional samples grown with the same germanium concentrations. Overlaid on the

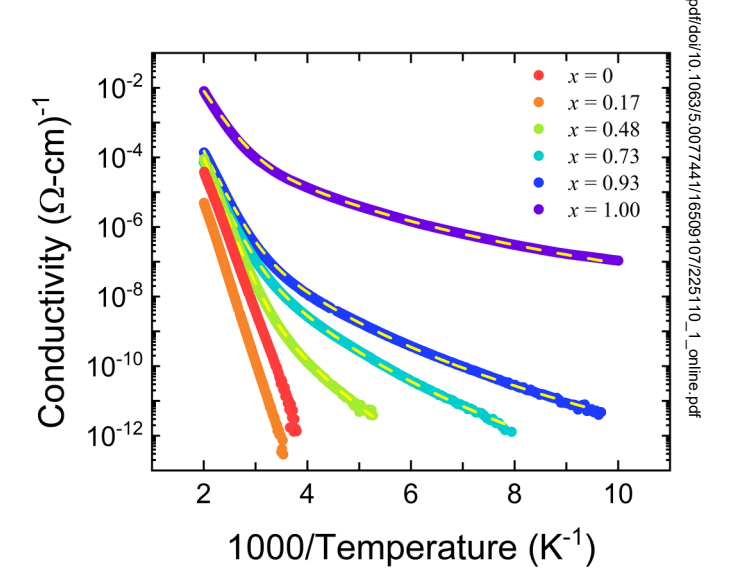


FIG. 2. Arrhenius plot of the dark conductivity of the a-Si_{1-x}Ge_x:H sample series for Ge content 0 < x < 1.0 for the full range of measured temperatures. Films with $x \le 0.17$ display anomalous hopping, while films with $x \ge 0.48$ exhibit multi-phonon hopping at low temperatures. The dashed yellow lines represent fits using the anomalous hopping and multi-phonon hopping expressions, as described in the text.

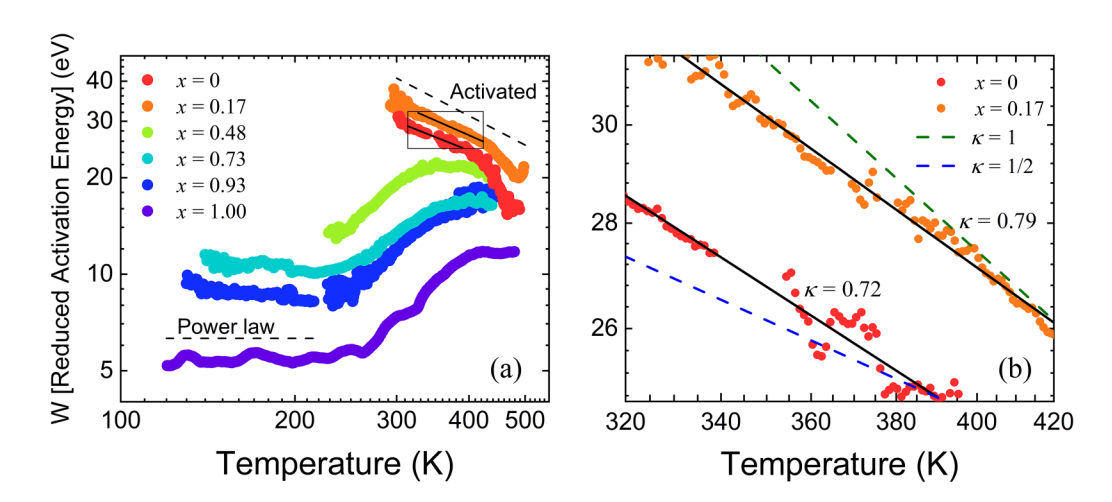


FIG. 3. (a) Log-log plot of the reduced activation energy against temperature for the a-Si_{1-x}Ge_x:H film series. (b) Expanded scale of the boxed region in (a) of the reduced activation energy for the x=0 and x=0.17 samples. The solid lines reflect the best fit curves of the form of Eq. (1) with $\kappa=0.72$ and $\kappa=0.79$, respectively. The green and blue dashed lines indicate the expected curves for slopes of $\kappa = 1.0$ and $\kappa = 1/2$, respectively.

plot are calculations of the reduced activation energy for conductivity temperature dependences of the form of Eq. (1), where $\kappa = 1$ (activated) and $\kappa = 0$ (power-law), as well as the line corresponding to the best fit (solid) for the x = 0 and x = 0.17 films.

As shown in Fig. 3(b), the conductivity temperature dependence for the a-Si:H and a-Si₈₃Ge₁₇:H films is inconsistent with the $\kappa = 1$ model curve and matches very closely with the $\kappa = 3/4$

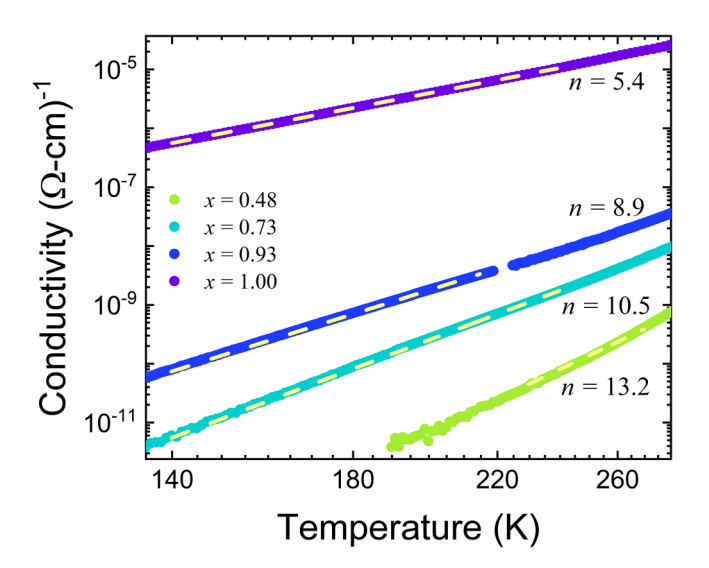


FIG. 4. Log-log plot of the dark conductivity vs temperature for the a-Si_{1-x}Ge_x: H film series with $x \ge 0.48$ in the low-temperature range. The linear behavior is consistent with an MPH type of conduction, in which case the slope value n is related to the average number of phonons involved in the hopping process. The dashed lines are fits to an MPH model as described in the text.

model curve found in previous studies, 15,16 specifically $\kappa = 0.72$ and $\kappa = 0.79$, respectively.

In general, we find $\kappa=0.75\pm0.05$, consistent with measurements on other amorphous semiconductors. ¹⁵ Although there is no generally accepted theoretical model for this conductivity temperature dependence, a model of conduction through the exponential band tails has been proposed to account for this anomalous hopping behavior in a-Si:H-based films. ¹⁵ In this case, the product of the rapidly increasing density of states in the exponential band tail with the decreasing thermal occupation due to the Fermi energy residing in the midgap yields charge transport occurring energy residing in the midgap yields charge transport occurring predominantly through localized states at a "transport energy" that is unconnected to a mobility edge.

ductivity studies is < 500 K, which is deliberately kept below the deposition temperature of 520 K in order to avoid irreversible changes in the electronic properties of the sample. deposition temperature of 520 K in order to avoid irreversible changes in the electronic properties of the samples. The downward kink in the reduced activation energy near 425 K for the x = 0 and x = 0.17 films in Fig. 3(a) reflects thermal equilibration effects¹⁵ x = 0.17 films in Fig. 3(a) reflects thermal equilibration effects¹⁵ and is not included in the fitting for κ values. For temperatures \bar{Q} below 275 K, the current levels are too low to be reliably measured.

Alloys with germanium content $x \ge 0.48$ show a reduced $\frac{1}{8}$ activation energy slope equal to zero at temperatures below 250 K, as shown in Fig. 3(a). This slope is characteristic of a power-law temperature-dependent conductivity of the type

$$\sigma(T) = \sigma_o^* \left(\frac{T}{T_o}\right)^n. \tag{3}$$

This relationship is confirmed by plotting the data from Fig. 2 on a log-log plot of σ against the temperature, as shown in Fig. 4. This behavior has been observed in non-hydrogenated a-Ge³¹ as well as amorphous carbon, 32,33 glasses containing transition metal ions, 34 and grain boundary states in nanocrystalline diamond.³⁵ Above ~300 K,

these films exhibit a reduced activation energy that increases with the temperature. As shown below, this may be due to a competition between a power-law temperature dependence and either an anomalous hopping or thermally activated conductivity in this temperature range.

IV. SEEBECK COEFFICIENT

The thermopower of the $a-Si_{1-x}Ge_x$:H thin-film samples was measured as a function of temperature using the apparatus and procedure described above. Figure 5(a) shows the raw thermopower data for a pure a-Si:H sample in a ΔV vs T plot. Each group of data points, connected by a line, represents a different average T, ranging from 310 to 480 K, and each data point within a group corresponds to a different ΔT value. All curves clearly display a negative slope over the entire temperature range examined. Similarly, a film with x=0.48, shown in Fig. 5(b), displays an induced voltage against temperature with a positive slope. In contrast, a film with x=0.73, shown in Fig. 5(c), displays a negative slope near room

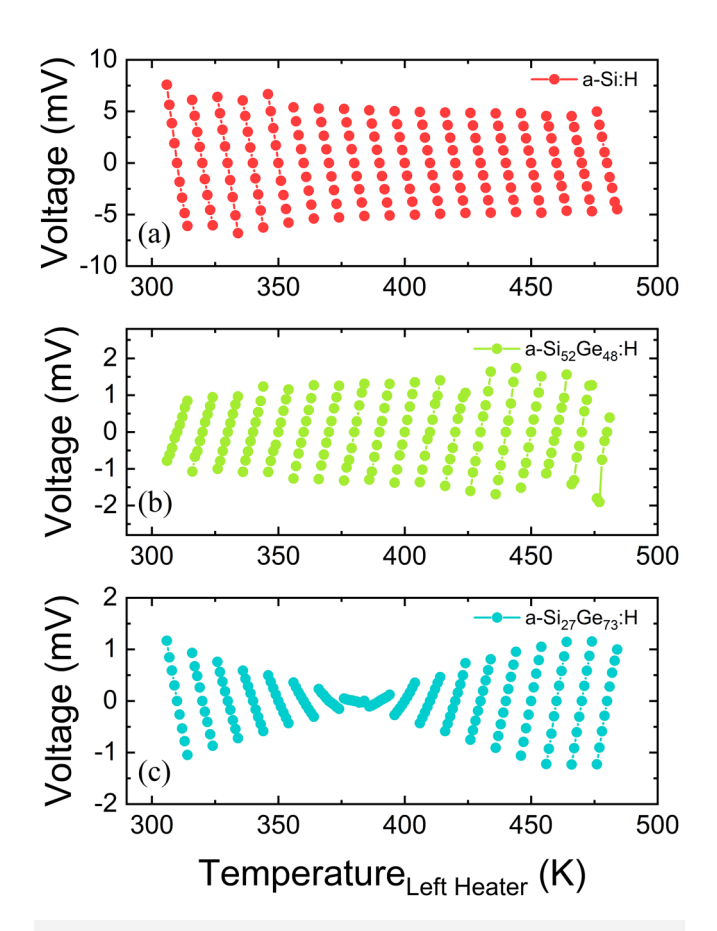


FIG. 5. Plots of the measured thermoelectrically induced voltage against temperature of the left heater (proportional to the gradient across the sample), recorded for increasing average temperatures, ranging from 310 to 480 K, for the (a) a-Si_{5.2}Ge₄₈:H, and (c) a-Si_{2.7}Ge₇₃:H films.

temperature, while above ~380 K, the slope switches to a positive value. This measurement procedure was repeated for all of the Si–Ge alloy films, with 0 < x < 1. The slopes of the plots of ΔV against ΔT in Fig. 5 yield the Seebeck coefficient [Eq. (2)], which is plotted in Fig. 6 against the average temperature for all the films investigated here. Similar behavior of the Seebeck coefficient temperature dependence was observed in other alloy films that were synthesized with the same Ge concentrations.

The data in Fig. 6 were fitted to the expression

$$S = \frac{k_B}{e} \left[\frac{E_S}{k_B T} + A \right],\tag{4}$$

where $\frac{E_S}{e}$ is the heat carried per charge carrier, and for electrons, it would be $E_T - E_F$, where E_T is the energy at which charge transport occurs and E_F is the Fermi energy, k_B is Boltzmann's constant, and A is the heat of transport constant. This last term accounts for

the carriers above E_T and is given by $A = \frac{\int_{\overline{k_B}T}^{E} \sigma(E)dE}{\int \sigma(E)dE}$, where $\sigma(E)$ is

the conductivity for single electron states at an energy E, ignoring correlation effects. For electrons, the integral extends from 0 to ∞ . If the density of states and mobility varies linearly with energy, then $A \sim 3$, though values as high as $A \sim 10$ have been reported. 36,37 A summary of the resulting activation energies and the fitted A values are listed in Sec. VI.

V. PHOTOCONDUCTIVITY

Photoconductivity provides information on the density of recombination centers in a sample, typically ascribed to dangling bond defects. The higher the density of dangling bonds, the lower the photoconductivity of a sample, as more photo-excited electrons are trapped in the defects. Figure 7 shows the measured photoconductivity of the a-Si_{1-x}Ge_x:H film series taken at room temperature for a fixed light intensity. The decrease in photoconductivity

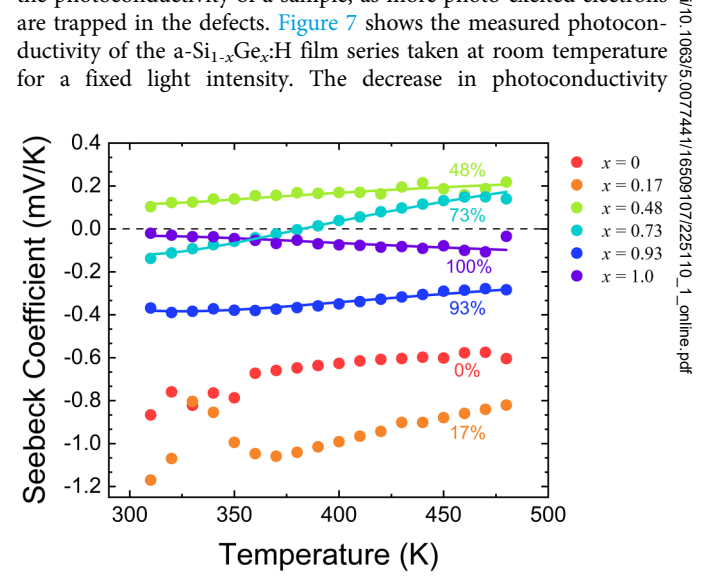


FIG. 6. Seebeck coefficient as a function of temperature for the a-Si_{1-x}Ge_xiH film series. A switch in the Seebeck coefficient sign is seen as a function of the temperature and Ge content. The solid lines for the $x \geq 0.48$ films are not a guide to the eye but fits using the dual-channel model described in the text.

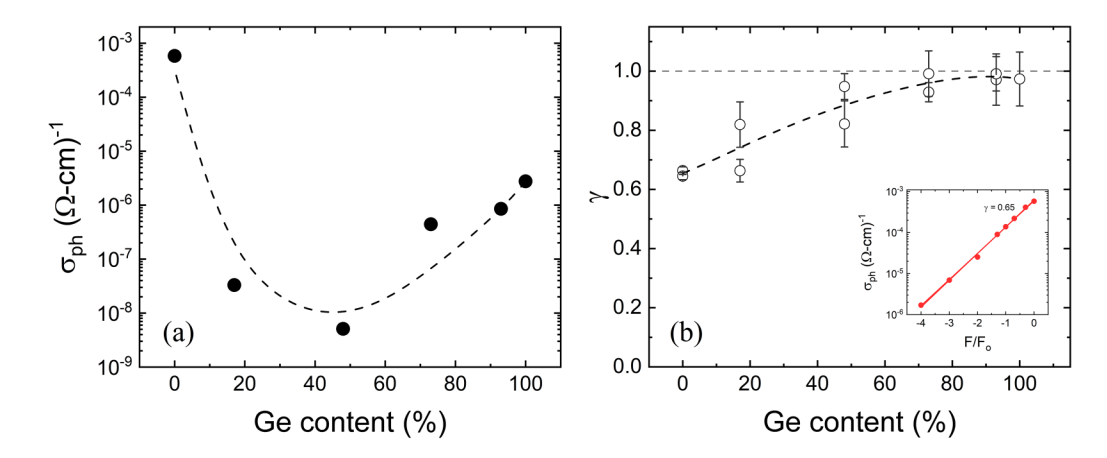


FIG. 7. (a) Plot of the photoconductivity of the a-Si_{1-x}Ge_x:H thin-film series at room temperature as a function of the Ge content. The dashed line serves as a visual guide. (b) Plot of the room temperature photoconductivity's light intensity power-law exponent γ against the Ge content of the a-Si_{1-x}Ge_xH alloy thin films. The power-law exponent is obtained from a log-log plot of the photoconductivity against light intensity, as shown in the inset for the a-Si:H film for which $\gamma \sim 0.65$.

between the a-Si:H and the a-Ge:H samples is attributed to the preference of H atoms to bond with Si rather than Ge, resulting in a large defect density stemming from dangling bonds on unhydrogenated Ge atoms. 38,39 Samples in the low- to mid-range of the Ge content display the lowest photoconductivity, most likely due to the presence of both Si and Ge dangling bonds in higher concentrations than in the pure a-Si:H and a-Ge:H samples. The photoconductivity σ_{ph} is given by $G \times \tau$, where G is the generation rate, proportional to the absorbed light intensity, and τ is the recombination lifetime. This lifetime is, in turn, inversely proportional to the density of recombination centers, which are presumed to be predominately dangling bond defects.⁴⁰ From these results, the density of defects N can be estimated for each sample, as listed in Table I.

The value of the photoconductivity is highly dependent on the light intensity used. As the light intensity is increased, the quasi-Fermi level adjusts, moving through the electron trapping states toward the conduction band, and more and more trapping states are converted into recombination centers. This effect can be described through a power-law relationship^{41,42} between the steady state photoconductivity σ_{ph} and the light power density,

$$\sigma_{ph} \propto F^{\gamma},$$
 (5)

where F is the light power density or irradiance, as shown in the inset in Fig. 7(b). This expression describes how the number of free carriers increases as the light power intensity used gets larger, while carriers increases as the light power intensity used gets larger, while more trap centers are converted into recombination centers. Different ranges of the exponent γ have been seen for different $\frac{1}{2}$ materials. For a-Si:H, values of $0.6 < \gamma < 0.9$ have been reported.⁴³ Direct recombination of photo-excited electron-hole pairs is characterized by $\gamma = 0.5$ (bimolecular recombination). In pairs is characterized by $\gamma=0.5$ (bimolecular recombination). In contrast, if one photo-excited charge carrier is trapped at a midgap defect, then $\gamma=1$ (monomolecular recombination). Al, 42 For these a-Si_{1-x}Ge_x:H thin-film samples, $\gamma\sim0.6$ for x<0.48 and transitions to $\gamma\sim1$ for higher Ge concentrations, as shown in Fig. 7(b). Will DISCUSSION

While the "mobility gap" model has been the dominant paradigm for understanding transport in amorphous semiconductors for the last 50 years. Al, 44 the recent observation of anomalous

for the last 50 years, ^{14,44} the recent observation of anomalous hopping behavior ^{15,16} challenges our understanding of charge transport in strongly disordered systems. Certainly, a simple, thermally activated expression appears to describe the conductivity temperature dependence, as shown in Fig. 8(a), where the data for an $a-Si_{83}Ge_{17}$:H alloy thin film yields a reasonable fit on an $\frac{\pi}{2}$ Arrhenius plot. Also shown in Fig. 8(a) is the same data plotted against $1/T^{0.79}$, and while close examination indicates a better fit to

TABLE I. Parameters used and obtained from fitting the conductivity data to an MPH model. The density of carriers is given by N, calculated from the defect density resulting from photoconductivity measurements. R is set to R = $1/N^{1/3}$. The localization radius α was obtained from an interpolation between reported values for a-Si:H and a-Ge:H.

Sample Si/Ge content	$N (\text{cm}^{-3})$	R (cm)	α (cm)	р	E_M (meV)	v _o (GHz)
a-Si ₅₂ Ge ₄₈ :H	1.1×10^{21}	1.2×10^{-7}	2.6×10^{-8}	14.2	74	131
a-Si ₂₇ Ge ₇₃ :H	1.3×10^{19}	7.0×10^{-8}	6.4×10^{-8}	11.5	48	103
a-Si ₇ Ge ₉₃ :H	6.8×10^{18}	5.1×10^{-7}	9.7×10^{-8}	9.9	9.5	22.0
a-Ge:H	2.1×10^{18}	9.6×10^{-7}	11×10^{-8}	6.4	9.2	47.9

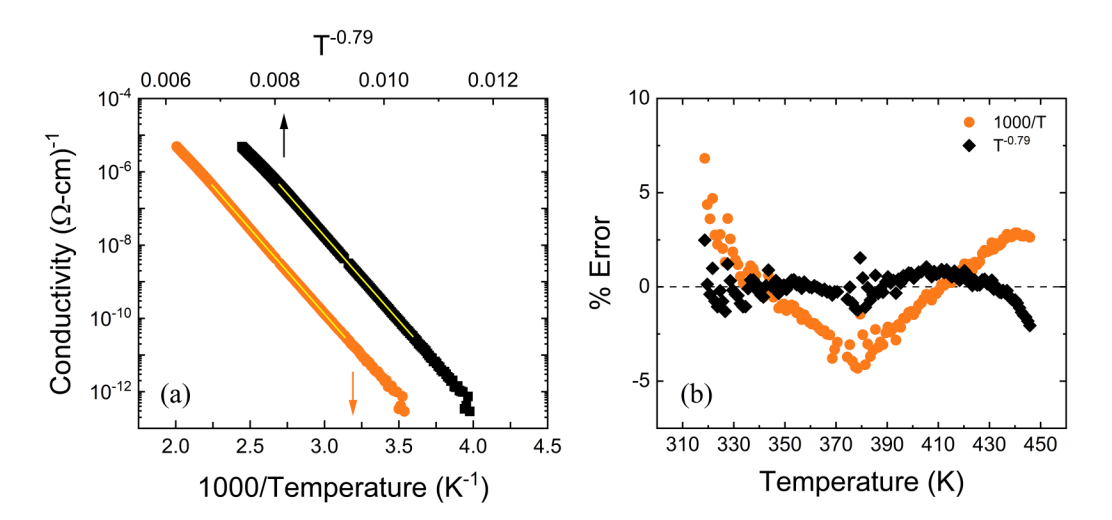


FIG. 8. (a) Plot of the dark conductivity of the a-Si₈₃Ge₁₇:H film against 1/T (gold) and 1/T^{0.79} (black). Straight lines (yellow) are overlaid on the data. (b) Plot of the deviations from fits of the data to a simple thermally activated (gold) and anomalous hopping (black) for the data in Fig. 8(a).

the data, the difference is subtle. In fact, the difference between a fit of the log-conductivity against 1/T and $1/T^{3/4}$ must be subtle, for if it were striking, it would have been noticed long ago. A plot of the percent difference between the data and the fit line for fits to 1/Tand $1/T^{0.79}$ shown in Fig. 8(b) indicates that the latter provides a more accurate description of the data. Note that the superior fit in Fig. 8 using $\kappa = 0.79$ is not simply a matter of adding an additional adjustable parameter to the fitting procedure. Rather, this exponent is experimentally determined from the reduced activation energy analysis procedure [Fig. 3(b)]. Measurements of a low-defect intrinsic c-Si wafer with the reduced activation energy analysis found a power-law exponent of $\kappa = 0.96$, consistent with the expected Arrhenius behavior.1

In addition to the observation that anomalous hopping behavior is observed in hydrogenated amorphous silicon-germanium alloy thin films, we also find that the conductivity below room temperature of films with higher germanium concentrations displays a power-law temperature dependence. Previous studies of nonhydrogenated a-Ge and a-SiGe have observed deviations from Arrhenius behavior, with charge transport at lower temperatures being attributed to a VRH mechanism, where the conductivity varies as Eq. (1) with $\kappa = 1/4$, 45,46 and for very low temperatures, to ES-VRH, where κ takes the value of ½. 46 A comparison between different temperature dependences of the a-Ge:H dark conductivity is presented in Fig. 9, including those corresponding to Mott-VRH and ES-VRH. Specifically, the comparison shows the conductivity data as a function of T^{-1} , $T^{-1/2}$, and $T^{-1/4}$, as well as a power-law temperature dependence (log(T)), for the low-temperature range. While a $T^{-1/4}$ appears to provide a reasonable fit to the data for a temperature range comparable to that of the power-law fit, as shown in Fig. 9(a), the percent error for the Mott-VRH expression, as well as that for an Arrhenius or Efros-Shklovskii-VRH temperature dependence, is significantly larger than for the power-law temperature dependence [Fig. 9(b)].

A power-law temperature dependence of the dc dark conductivity has been attributed to charge transport via multi-phonon by hopping. In such a process, charges reside in the weakly localized defect states and preferentially couple to phonons with wavelengths bond defects, this localization length would be on the order of $\frac{1}{10}$. The hopping process, therefore, involves long-wavelength low-energy acoustic phonons, and consequently, multiple phonons must participate in a single hop event. If p phonons are required to $\frac{1}{10}$ must participate in a single hop event. If p phonons are required to must participate in a single hop event. If p phonons are required to initiate a transition from one defect state to another, then the hopping frequency will depend on p factors of the Bose-Einstein distribution function, which would lead to a power-law temperature dependence when $hv_o \ll kT$.

The hopping conductivity is given by the expression $\frac{48}{6k_BT}$ $\sigma = \frac{N(eR)^2}{6k_BT}\Gamma$, (6) where N is the density of localized carriers (equivalent to the number of occupied defect states), e is the electron charge, R is the hopping distance, and Γ is the hopping rate. This rate has been $\frac{1}{8}$

$$\sigma = \frac{N(eR)^2}{6k_BT}\Gamma,\tag{6}$$

hopping distance, and Γ is the hopping rate. This rate has been \ddot{g} determined by Robertson and Friedman^{47,48} and can be expressed

$$\Gamma = v_o \exp\left[-\frac{2R}{\alpha}\right] \exp\left[-\frac{E_M}{hv_o}\right] \left(\frac{E_M}{hv_o}\right)^p [n_{BE}(v_o)]^p, \tag{7}$$

where α is the localization radius, E_M is a measure of the electronphonon coupling, $n_{BE}(v_o)$ is the Bose-Einstein distribution for phonons of frequency v_0 , and p is the number of phonons needed for the hopping to take place. In the regime of $hv_0 \ll k_B T$, Eq. (7) can be Taylor expanded into a power law of the form of Eq. (3), with n = p - 1.

The low-temperature range of all samples with $x \ge 0.48$ was fitted using Eqs. (6) and (7), indicated by the dashed lines overlaid with the data in Fig. 4. The fitting range was chosen to avoid contributions from other conduction mechanisms, as described below. The factors v_o and E_M were kept as free parameters given that we do not possess a procedure to accurately estimate them. From a set of photoconductivity measurements, we were able to determine the density of defects. In MPH, transport is expected to take place through these defect states; therefore, we can assume that they are described by N. The hopping distance between states R was estimated as $R = 1/N^{1/3}$. From the power-law fittings shown in Fig. 4, we can determine p = n + 1. The localization radius α of dangling bond defects in a-Si:H and a-Ge:H has been found to be 0.5 and 1.1 nm, ⁴⁹ respectively. We interpolate the corresponding values for samples with $0.48 \le x \le 0.93$, using a non-monotonic interpolating function determined by Street and co-workers⁴⁰ for a-Si_{1-x}Ge_x: H samples as a function of their Ge concentration. These authors considered the distance between an electron-hole pair and the nearest dangling bond (critical transfer radius) R_c , which is expected to be proportional to α . The parameter values used while fitting, as well as the free fitting parameters v_o and E_M , are given in Table I.

The obtained E_M values are between 9–80 meV and scale inversely with the Ge content of the samples. These values are consistent with those calculated by Drabold^{50,51} using first-principles computer simulations for low frequency phonons in an a-Si model. The parameter ν_o was found to be on the order of ~0.1 THz for all the samples, which corresponds to a phonon temperature of ~5 K. This value of phonon frequency agrees with Shimakawa's estimation for MPH transport through dangling bonds in a-Ge.³¹

At temperatures at and above room temperature, the multiphonon hopping expression is unable to account for the observed conductivity temperature dependence. However, when the expression in Eq. (6), using Eq. (7) for Γ and the parameters from Table I, is combined with Eq. (1), with $\kappa = 3/4$, the resulting expression provides a satisfactory fit to the data over the entire

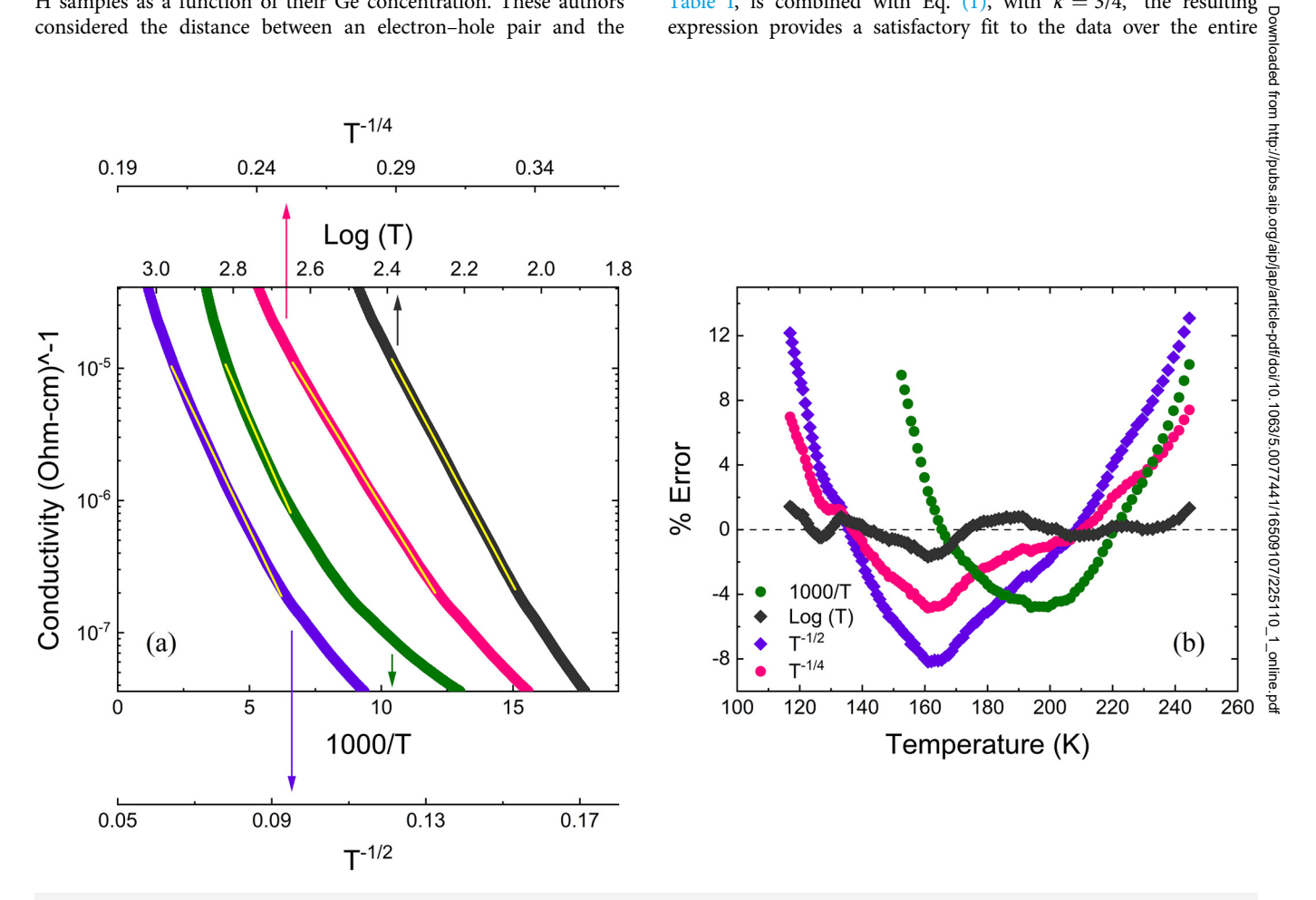


FIG. 9. (a) Plot of the log of the dark conductivity of the a-Ge:H film for temperatures below 250 K when plotted against 1000/T (green circles), $T^{-1/2}$ (purple diamonds), $\log(T)$ (black diamonds), and $T^{-1/4}$ (pink circles). The best fit lines (yellow) of each are overlaid on the data. (b) Plot of the percent differences from fits of the conductivity temperature dependence [Eq. (1)] for $\kappa = 1.0$ (green diamonds), $\kappa = 1/2$ (purple diamonds), $\kappa = 1/4$ (pink circles) and for a power-law temperature dependence (black diamonds). The percent error shows systematic variations with temperature for all temperature dependences, except for the power-law fit, for which the percent error fluctuates randomly about 0%, consistent with the Zabrodskii reduced activation energy analysis.

temperature range investigated, as indicated by the dashed lines in Fig. 2. For the x=0.48 film, the anomalous hopping expression provides a better description of the high temperature data than a simple Arrhenius expression, while for $x\geq 0.73$, the fits to the observed data are comparable for either expression. We thus cannot rule out that the conductivity temperature dependence for the higher Ge content alloys has a simple thermally activated component.

Using a model of MPH conductivity at low temperatures combined with anomalous hopping at high temperatures, the fractional conductivity due to each transport mechanism is computed as a function of temperature. We can define the fractional conductivity as σ_i/σ_{tot} , where i is either the contribution to the conductivity due to anomalous hopping or MPH conduction, as shown in Fig. 10. For all samples, there is a considerable contribution from MPH at temperatures as high as 400 K. This is indicative of the existence of conduction through dangling bond defects in all samples, even for temperatures above room temperature. The temperature at which the transition between conduction mechanisms happens (MPH to anomalous hopping) generally increases as the Ge content.

Thermopower measurements of the a-Si_{1-x}Ge_x:H sample series show a transition from negative to positive Seebeck coefficient as a function of Ge content and temperature. The Fermi energy for these samples, as seen from the electrical dark conductivity analysis, resides in a continuous DOS where according to the MPH model, charge transport takes place. The Seebeck coefficient in

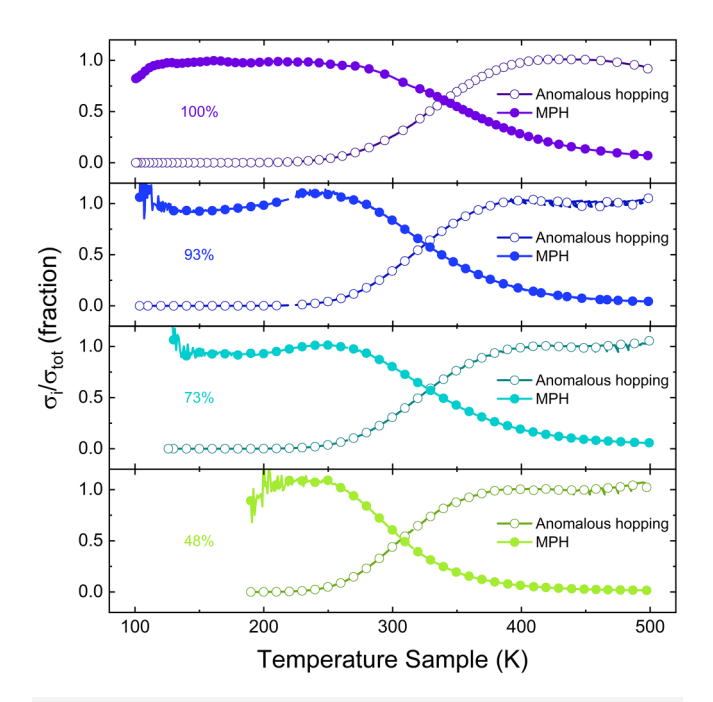


FIG. 10. Calculated fractional conductivity, σ_i/σ_{tot} for each electronic transport mechanism (anomalous hopping and MPH) plotted against temperature for 100–500 K. All samples show a mix of conduction mechanisms even for temperatures as high as 400 K. Only every fifth data point has been displayed for clarity.

such cases is better described through a metal-like thermopower⁵² where the Seebeck coefficient is directly proportional to the derivative of the DOS at the Fermi level. Therefore, a change in the Seebeck coefficient sign may be interpreted as a result of the Fermi level moving within the midgap populated by dangling bond states, rather than due to a change in the carrier type in band-to-band transport.

According to the dark conductivity model described above, the transport mechanism in these samples can be considered as a dual-channel system, with two parallel temperature-variable resistors, one related to anomalous hopping and the second, to MPH. The cross section of the resistor corresponding to anomalous hopping is larger than that of MPH at high temperatures so that the current mostly flows through the anomalous hopping channel at those temperatures. As the temperature decreases, the resistances vary until the MPH channel ends up being the predominant charge transport mechanism at lower temperatures. At intermediate temperatures, the resistors' cross sections, and, therefore, their resistances, are comparable to each other, and current flows through both channels.

The resulting thermopower for these series of samples is determined by the relative contribution of each conduction channel (anomalous hopping and MPH), as

$$S = \frac{S_{AH} \times \sigma_{AH} + S_{MPH} \times \sigma_{MPH}}{\sigma_{AH} + \sigma_{MPH}},$$
 (8)

where S_{AH} and σ_{AH} are the Seebeck coefficient and dark conductivity contributions due to an anomalous hopping conduction, respectively, and S_{MPH} and σ_{MPH} are those corresponding to MPH. We can understand Eq. (8) as if the total thermopower S for this system was determined by the number of charge carriers in each phase (anomalous hopping or MPH) and their mobilities.

phase (anomalous hopping or MPH) and their mobilities.

Given the limited temperature range for which there is data available and the small contribution coming from the MPH at high temperatures, we can assume a negligible temperature dependence in S_{MPH} for the $310 \le T \le 480$ K range. We, therefore, assume no temperature dependence in S_{MPH} . S_{AH} corresponds to transport between the valence band edge and the states within the conduction bandtail. Due to its similarity to an activated transport mechanism, we assume that its Seebeck coefficient will be very similar to that presented in Eq. (4), where E_S takes the values presented in Table II for samples with $x \ge 0.48$. The two adjustable fitting parameters are S_{MPH} and the heat of transport constant A.

The solid lines in Fig. 6 correspond to the calculated thermopower for the $a-Si_{1-x}Ge_x$:H samples with $x \ge 0.48$ using the dual-channel expression in Eq. (8), which successfully describes the thermopower temperature dependence. The parameters used to reproduce the model are listed in Table II. Notice that to minimize the number of fitting parameters, the E_S values were obtained from fitting the thermopower to an activated conduction, which does not accurately describe the data, but yields a reasonable value for the activation energy. The change in sign with temperature of the Seebeck coefficient for the x=0.73 alloy film appears to result from a large negative activation energy E_S and a large, positive heat of transport constant A. While the heat of transport constant as defined above can never be less than 0, there are other constants

Sample	E_S (eV)	A	S_{MPH} (mV/K)
a-Si ₅₂ Ge ₄₈ :H	-0.09	4.6	1.3×10^{-1}
a-Si ₂₇ Ge ₇₃ :H a-Si ₇ Ge ₉₃ :H	-0.31 -0.15	9.7 0.4	-9.4×10^{-2} -3.4×10^{-1}
a-Ge:H	0.07	-2.9	-3.5×10^{-2}

that enter into the temperature dependence of the Seebeck coefficient, such as the temperature dependence of the bandgap, which can lead to a negative A.53 More studies of the thermopower and the density of states of the alloy thin films, particularly for high germanium concentrations, would help elucidate the nature of the heat of transport term.

From these results, we can affirm that a dual-channel conduction picture is in agreement with our experimental data. The two channels are due to anomalous hopping, which is inversely dependent with temperature, more prevalent at high temperatures, and an MPH mechanism, which either varies slowly with temperature or is temperature independent.

One surprising result of this analysis is the contribution of a power-law temperature dependence to the conductivity for temperatures at or even above room temperature. We are unaware of any published reports of MPH conduction at such high temperatures, with nearly all cases of MPH being observed only below room temperature. At higher temperatures, optical phonons with higher energies should be present, obviating the need for a multi-phonon process. Moreover, as shown in Fig. 4, the a-Si₅₂Ge₄₈:H alloy requires as many as fourteen phonons in order to facilitate hops between states. A larger number of phonons required for hopping would suggest that transport between localized states is more difficult, either due to a large separation between defect states or a lower electron-phonon coupling, or a combination of the two. However, the a-Si₅₂Ge₄₈:H alloy has the lowest photoconductivity value [Fig. 7(a)] of the films studied here, suggesting a high density of dangling bond defects. The electron-phonon coupling fitting parameter for this film is similarly the largest of the alloys displaying a power-law temperature dependence (Table I). It is possible that multi-phonon hopping is not, in fact, the charge transport mechanism responsible for the observed power-law temperature dependence in these and possibly other amorphous semiconductors, though we do not, at present, know of an alternative mechanism.

VII. CONCLUSIONS

Analysis of the temperature dependence of the dark conductivity for a series of a-Si_{1-x}Ge_x:H thin films finds that for Si rich samples (x < 0.20), the conductivity is well described by an anomalous hopping expression, while for higher Ge concentrations, the dark conductivity is best described by a power-law temperature dependence below 250 K, and anomalous hopping or simple thermal activation at higher temperatures. Studies of the Seebeck coefficient for these films is also consistent with a dual-channel model, with charge transport occurring through a relatively high density of midgap defects, likely associated with Ge dangling bonds. These studies suggest that electronic conduction in amorphous semiconductors involves charge transport via hopping through localized states (either in exponential band tails or midgap dangling bonds) rather than thermal excitation to extended states above a mobility edge. Additional studies of the sensitivity of these results to the deposition conditions under which the films are synthesized, as well as a wider range of amorphous semiconductors, are warranted.

ACKNOWLEDGMENTS

We gratefully acknowledge helpful discussions with David Drabold and Boris Shklovskii. This work was supported by NSF Grant No. DMR1608937, the Minnesota Environment and Natural Resources Trust Fund (ML 2016, Chap. 186, Sec. 2, Subdivision 07b), and the University of Minnesota. Parts of this work were carried out in the Characterization Facility, University of a Minnesota, which receives partial support from the NSF through carried out in the Characterization Facility, University of the MRSEC (Award No. DMR-2011401) and the NNCI (Award

the MRSEC (Award No. DMR-2011401) and the NNCI (Award No. ECCS-2025124) programs. Portions of this work were conducted in the Minnesota Nano Center, which is supported by the National Science Foundation through the National Nano Coordinated Infrastructure Network (NNCI) under Award No. ECCS-1542202.

AUTHOR DECLARATIONS

Conflict of Interest

The authors have no conflicts to disclose.

Author Contributions

L. Stolik: Formal analysis (lead); Investigation (lead); Methodology (lead); Writing – original draft (equal); Writing – review & editing (equal). M. A. Eslamisaray: Investigation (supporting); Methodology (supporting); Writing – original draft (equal). E. Nguyen: Unvestigation (supporting); Methodology (supporting); Writing – writing – original draft (equal). E. Nguyen: Nethodology (supporting); Writing – Writi (equal); Writing – review & editing (equal). E. Nguyen: 1782 [Investigation (supporting); Methodology (supporting); Writing – 1782 [Investigation (supporting)]. U. R. Kortshagen: Funding acquisition (equal); Writing – original draft (supporting); Writing – review & editing (equal). J. Kakalios: Funding acquisition (equal); Project administration (equal); Supervision (equal); Writing - original draft (equal); Writing - review & 🖫 editing (equal).

DATA AVAILABILITY

The data that support the findings of this study are available from the corresponding author upon reasonable request.

REFERENCES

¹N. Koshida, Device Applications of Silicon Nanocrystals and Nanostructures (Springer Science & Business Media, 2008).

²R. Street, Technology and Applications of Amorphous Silicon (Springer Science & Business Media, 1999), Vol. 37.

- ³A. Gusev and A. Rempel, Nanocrystalline Materials (Cambridge International Science Publishing, 2004).
- ⁴A. D. Franklin, Science **349**, 6249 (2015).
- ⁵I. Shimizu, "Photoreceptor and vidicon," MRS Proc. **49**, 395 (1985).
- ⁶D. M. Pai and B. E. Springett, Rev. Mod. Phys. **65**, 163 (1993).
- ⁷J. Rowlands and S. Kasap, Phys. Today **50**, 24 (1997).
- ⁸M. Moll, J. Adey, A. Al-Ajili, G. Alfieri, P. Allport, M. Artuso, S. Assouak, B. Avset, L. Barabash, A. Barcz, and R. Bates, Nucl. Instrum. Methods Phys. Res., Sect. A 546, 99 (2005).
- ⁹M. Moll, IEEE Trans. Nucl. Sci. **65**, 1561 (2018).
- ¹⁰N. Kishimoto, H. Amekura, K. Kono, and C. G. Lee, J. Nucl. Mater. 258–263, 1908 (1998).
- ¹¹A. Shah, P. Torres, R. Tscharner, N. Wyrsch, and H. Keppner, Science 285, 692 (1999).
- 12J. Yang, A. Banerjee, and S. Guha, Sol. Energy Mater. Sol. Cells 78, 597 (2003). ¹³S. Guha, Multijunction Solar Cells and Modules in Technology and Applications of Amorphous Silicon (Springer, 2000), p. 252 in Ref. [2].
- ⁴N. F. Mott, Adv. Phys. **16**, 49 (1967).
- 15 K. Bodurtha and J. Kakalios, J. Appl. Phys. 118, 215103 (2015).
- 16B. J. Western, M. S. Harcrow, V. C. Lopes, A. J. Syllaios, U. Philipose, C. L. Littler, S. Andrews, T. Chang, and J. Hong, J. Non-Cryst. Solids 564, 120845 (2021).
- 17N. Marković, C. Christiansen, D. E. Grupp, A. M. Mack, G. Martinez-Arizala, and A. M. Goldman, Phys. Rev. B 62, 2195 (2000).
- ¹⁸I. Shlimak, S. I. Khondaker, M. Pepper, and D. A. Ritchie, Phys. Rev. B 61, 7253 (2000).
- 19K. M. Mertes, H. Zheng, S. A. Vitkalov, M. P. Sarachik, and T. M. Klapwijk, Phys. Rev. B 63, 041101 (2001).
- ²⁰C. J. Adkins and E. G. Astrakharchik, J. Phys.: Condens. Matter 10, 6651 (1998). 21 D. Van der Putten, J. T. Moonen, H. B. Brom, J. C. M. Brokken-Zijp, and
- M. A. J. Michels, Phys. Rev. Lett. 69, 494 (1992). 22A. Zabet-Khosousi, P.-E. Trudeau, Y. Suganuma, A.-A. Dhirani, and B. Statt, Phys. Rev. Lett. 96, 156403 (2006).
- ²³A. J. Houtepen, D. Kockmann, and D. Vanmaekelbergh, Nano Lett. **8**, 3516
- ²⁴D. Hauschild, R. Fischer, and W. Fuhs, Phys. Status Solidi B **102**, 563 (1980).
- 25_{D. L. Staebler and C. R. Wronski, Appl. Phys. Lett. 31, 292 (1977); J. Appl.} Phys. 51, 3262 (1980).
- ²⁶M. Tanielian, Philos. Mag. B **45**, 435 (1982).

- ²⁷A. G. Zabrodskii and I. S. Shlimak, Sov. Phys. Semicond. 9, 391 (1975).
- 28 A. L. Efros and B. I. Shklovskii, J. Phys. C: Solid State Phys. 8, L49 (1975).
- ²⁹N. F. Mott, J. Non-Cryst. Solids **1**, 1 (1968).
- 30 H. M. Dyalsingh and J. Kakalios, Phys. Rev. B 54, 7630 (1996).
- 31 K. Shimakawa, Phys. Rev. B 39, 12933 (1989).
- 32 K. Shimakawa and K. Miyake, Phys. Rev. Lett. 61, 994 (1988).
- 33K. Shimakawa and K. Miyake, Phys. Rev. B 39, 7578 (1989).
- 34K. Shimakawa, Philos. Mag. B 60(3), 377 (1989).
- 35 F. Cleri, P. Keblinski, L. Colombo, D. Wolf, and S. R. Phillpot, Europhys. Lett. 46, 671 (1999).
- 36R. Callaerts, P. Nagels, and M. Denayer, Phys. Lett. A 38, 15 (1972).
- ³⁷S. A. Baily and D. Emin, Phys. Rev. B 73, 165211 (2006).
- ³⁸A. Morimoto, T. Miura, M. Kumeda, and T. Shimizu, Jpn. J. Appl. Phys. 20,
- 39 M. Kumeda, Y. Tsujimura, Y. Yonezawa, A. Morimoto, and T. Shimizu, Solid State Commun. 55, 409 (1985).
- 40 R. A. Street, C. C. Tsai, M. Stutzmann, and J. Kakalios, Philos. Mag. B 56, 289
- 42C. Main and A. E. Owen, in *Electronic and Structural Properties of Amorphous Emiconductors*, edited by P. G. LeComber, and J. Mort (Academic Press, 1973), ⁴²C. Main and A. E. Owen, in *Electronic and Structural Properties of Amorphous*
- p. 527. $^{\bf 43}$ J. Mort and D. M. Pai, Photoconductivity and Related Phenomena (Elsevier/ North-Holland, 1976).
- 44M. H. Cohen, H. Fritzsche, and S. R. Ovshinsky, Phys. Rev. Lett. 22, 1065 (1969).
- 1969).

 45S. C. Agarwal, S. Guha, and K. L. Narasimhan, J. Non-Cryst. Solids 18, 429 (1975).

 46N. Aoki, K. Nara, and Y. Ochiai, Phys. Status Solidi B 218, 5 (2000).

 47N. Robertson and L. Friedman, Philos. Mag. 33, 753 (1976).

 48N. Robertson and L. Friedman, Philos. Mag. 36, 1013 (1977).

 49M. Stutzmann and J. Stuke, Solid State Commun. 47, 635 (1983).

 50K. Prasai, P. Biswas, and D. A. Drabold, Semicond. Sci. Technol. 31, 073002 (2016).

 51R. Atta-Fynn, P. Biswas, and D. A. Drabold, Phys. Rev. B 69, 245204 (2004).

 52I. Zvyagin, "The hopping thermopower," in Hopping Transport in Solids (North-Holland, 1991), Vol. 28, p. 143.

 53D.-K. Ko and C. B. Murray, ACS Nano 5, 4810 (2011).